Characterization of identification errors and uses in localization of poor modal correlation

Guillaume Martin [a,b,*], Etienne Balmes [a,b], Thierry Chancelier [c]

[a] Arts et Metiers ParisTech, PIMM, 151 Boulevard de l'Hopital, 75013 Paris, France
[b] SDTools, 44 rue Vergniaud, 75013 Paris, France
[c] Chassis Brakes International, 126 rue de Stalingrad, 93700, Drancy, France

Keywords:
Modal assurance criterion
Identification error
Localization of poor correlation

A B S T R A C T

While modal identification is a mature subject, very few studies address the characterization of errors associated with components of a mode shape. This is particularly important in test/analysis correlation procedures, where the Modal Assurance Criterion is used to pair modes and to localize at which sensors discrepancies occur. Poor correlation is usually attributed to modeling errors, but clearly identification errors also occur. In particular with 3D Scanning Laser Doppler Vibrometer measurement, many transfer functions are measured. As a result individual validation of each measurement cannot be performed manually in a reasonable time frame and a notable fraction of measurements is expected to be fairly noisy leading to poor identification of the associated mode shape components.

The paper first addresses measurements and introduces multiple criteria. The *error* measures the difference between test and synthesized transfer functions around each resonance and can be used to localize poorly identified modal components. For intermediate error values, diagnostic of the origin of the error is needed. The *level* evaluates the transfer function amplitude in the vicinity of a given mode and can be used to eliminate sensors with low responses. A *Noise Over Signal* indicator, product of error and level, is then shown to be relevant to detect poorly excited modes and errors due to modal property shifts between test batches. Finally, a *contribution* is introduced to evaluate the visibility of a mode in each transfer. Using tests on a drum brake component, these indicators are shown to provide relevant insight into the quality of measurements.

In a second part, test/analysis correlation is addressed with a focus on the localization of sources of poor mode shape correlation. The MACCo algorithm, which sorts sensors by the impact of their removal on a MAC computation, is shown to be particularly relevant. Combined with the *error* it avoids keeping erroneous modal components. Applied after removal of poor modal components, it provides spatial maps of poor correlation, which help localizing mode shape correlation errors and thus prepare the selection of model changes in updating procedures.

* Corresponding author at: Arts et Metiers ParisTech, PIMM, 151 Boulevard de l'Hopital, 75013 Paris, France.
E-mail address: balmes@sdtools.com (E. Balmes).

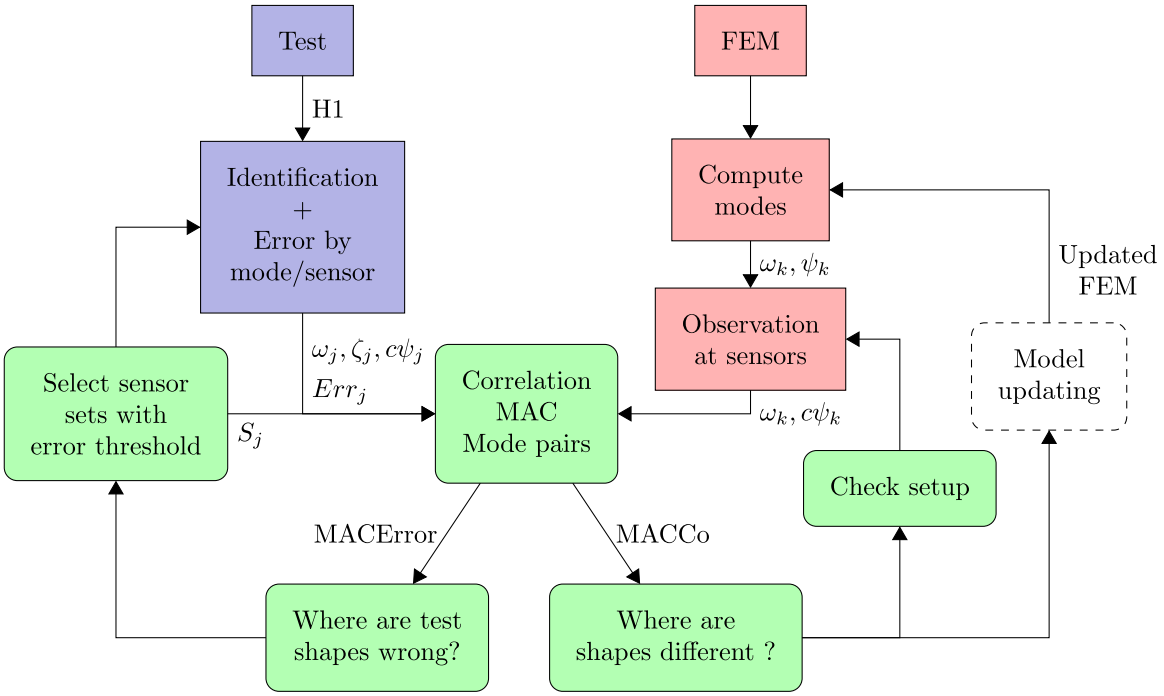

Fig. 1. Correlation evaluation during model updating process.

1. Introduction

Major reasons to perform modal testing are to understand the experimental behavior of a mechanical system and often to evaluate the correlation between test and analysis. The Modal Assurance Criterion (MAC) [1] is generally used for such correlation. It allows pairing of test and analysis (usually Finite Element Model (FEM)) mode shapes and provides a quantitative measurement of the difference between test and analysis. In most applications the motivation for the test is to help in the diagnosis of modeling errors and improvement of model parameters through updating [2].

Fig. 1 summarizes the use of the MAC correlation criterion in the model updating process used in this paper. On the one hand, data from test measurements are used to identify modes providing experimental frequencies ω_j, damping coefficients ζ_j and mode shapes $c\psi_j$. On the other hand, computation of the FEM provides numerical frequencies ω_k and mode shapes ψ_k, which need then to be observed at sensors, leading to $c\psi_k$. Identified and observed numerical mode shapes are then compared with the MAC and after pairing give correlation levels per mode pair. This presentation clearly highlights the fact that poor correlation can come from modeling errors, answering the question of where mode shapes are different as usually considered in updating processes, but also from test, thus answering the question of where test shapes are badly identified and not relevant. The objective of the work presented here is therefore to introduce and illustrate strategies for test error quantification and use in poor sensor localization.

Test errors may have different origins. Product variability can play a major role in updating processes and correlation analysis [3–5] but they will not be addressed. Test variability (loading variability, temperature evolution during test,…) are typically controlled through reproducibility tests. Methods involving bootstrap strategies [6,7] can be used to obtain uncertainty on identified parameters from repeated measurements. One important interest of these methods is that no assumption is made on the statistical law, but the major drawback is that all measurements must be saved (no averaging). Comparable results can be achieved using Monte Carlo methods [8] or Maximum Likelihood identification [9,10], but assuming a normal distribution of the measured response. In all of these cases, it is useful to note that any bias introduced by the chosen identification method has uncontrolled effects [7].

Illustrations of the proposed methods are based on 3D scanning laser Doppler vibrometer (3D-SLDV) measurements routinely used by Chassis Brakes International in the model validation process where brake components and assemblies are tested and correlated with FEM. The retained test case is detailed in Section 2.

The first focus of this paper is on a quantification of identification error, rather than building of an uncertainty model for identified parameters. After a description in Section 2 of the test case used as illustration, the identification procedure and notations used in the paper are presented in Section 3.1. An identification error is defined, in Section 3.2, by computing, for each mode and each sensor, the norm of the difference between measured and synthesized transfer functions around the resonance frequency. This criterion does not imply the need to use stochastic methods to estimate uncertainty bounds on modal parameters [9,10] and is as a result more easily used. Three additional indicators, level, contribution, and Noise Over

Signal are then introduced to help sorting measurements and in the diagnostic of non-relevant modal contributions. Taking identification results obtained using the pole tuning strategy [11] of the Structural Dynamics Toolbox [12] for MATLAB, these criteria are shown to allow proper diagnostic of measurement problems and the definition of sensor sets retaining reliably measured components of each mode shape.

The second paper contribution is an analysis, in Section 4, of strategies used to build valid sensor sets for different modes. When finding an intermediate correlation for mode pairs, topology correlation errors may first have to be corrected as discussed in Section 4.1. The second step is clearly a localization problem, or need to find which sensors lead to poor correlation. This need was identified very early and led to the CoMAC [13] and eCoMAC [14] criteria. These two approaches assume the identification to be correct. The COMEF [15] tends to minimize error detection at low amplitude sensors, which are more likely to be noisy. All of these methods need multiple modes and provide sensor sorting that ignores the fact that a given sensor may properly measure only some modes, thus implying that each mode has a different valid sensor set. The COrthog criterion [16] sorts discrepant DOFs for each paired mode introducing the notion of sensor sets differing for each mode, which is more deeply developed in [17] where low amplitude responses were removed for each mode. An interesting MAC variation technique, leading to global or per mode sensor sorting, was proposed in [18] and is implemented as MACCo in [12]. These methods are discussed in Section 4.2.

The initial MACCo algorithm characterizes sensors leading to poor correlation and provides a localization process to see where the model contains a poor mode shape. This corresponds to an *a posteriori* localization of correlation discrepancies. The identification error, being computed before correlation, provides *a priori* estimates of poor sensors, which can be used to define, for each mode, sets of accurately identified sensors. Discarding incorrectly identified components of the mode shape improves correlation by decreasing the test errors. Applications of these algorithms are detailed in Sections 4.3 and 4.4. Conclusions and perspectives are finally provided in Section 5.

2. Test setup and associated FEM

Throughout the paper results are shown for a drum brake part: a press-formed plate assembled with rivets to a cable guide, shown in Fig. 2 left. To be as close as possible to free-free boundary conditions, the plate is suspended with fishing lines. Different impact locations were tested and the one retained provides a good average modal controllability in the frequency range of interest.

Measurements are performed by a 3D-SLDV (3D-SLDV PSV-400 from Polytec). Fig. 3 left shows the experimental wireframe composed of 493 points associated with 1479 transfer functions (3 sensors in X Y and Z directions for each point). For every points, the responses to 8 impacts are measured and the transfer functions are obtained with the classical $H1$

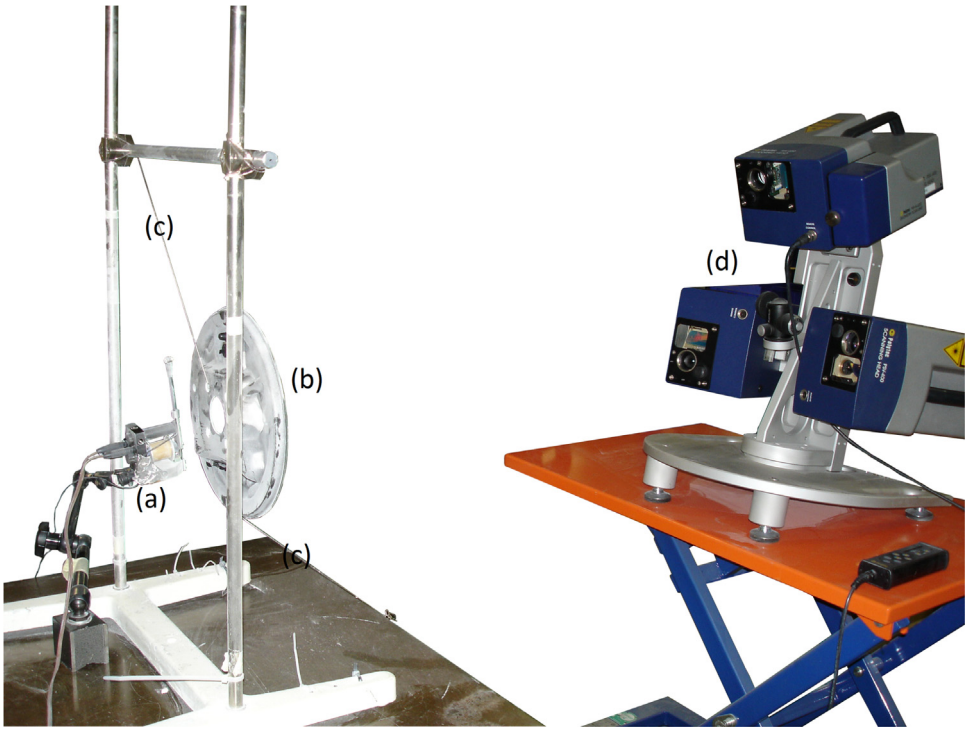

Fig. 2. Test setup: (a) Automated impact hammer, (b) measured brake plate, (c) fishing lines, (d) 3D-SLDV.

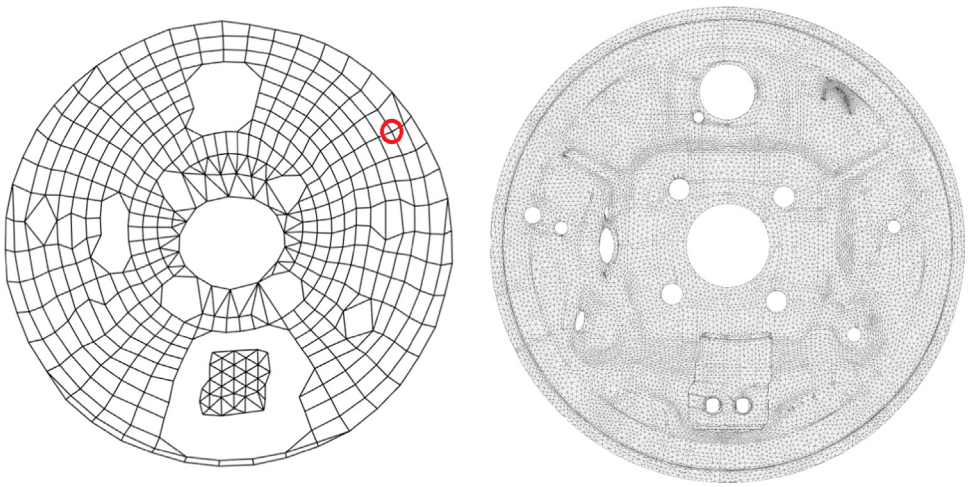

Fig. 3. Test configuration with automated impact and 3D scanning laser vibrometer measurements: test wireframe with impact hammer location in red (left) and Finite Element Model (FEM) (right).

estimator

$$H_1(\omega) = S_{yf}(\omega)S_{ff}(\omega)^{-1} \tag{1}$$

where S_{yf} is the cross power spectrum between the output displacements and the input force, and S_{ff} the auto power spectrum of the input force. Coherence was quite good even though it was not properly saved and could not be exploited. Individual validation of 1479 transfer functions cannot be performed manually in a reasonable time frame and a notable fraction of measurements is expected to be fairly noisy. The large number of measurements and the existence of poor sensitivity in certain directions augment the need to automatically determine accurate sensor sets, but the procedures that will be proposed are clearly also relevant in accelerometer or roving hammer tests.

The correlation will be evaluated with the finite element model shown in Fig. 3 right. This model is finely meshed with a characteristic length of 2.7 mm, 183,800 nodes and 93,253 elements. Computation of the first 50 modes takes 131 s on a standard workstation.

3. Identification error and other criteria on measured transfers

While many identification procedures exist, see for example the books [19,20], associated errors are rarely quantified. For example, it is common practice to choose a mode shape within a set of possibilities in a stabilization diagram. This selected mode becomes a user based reference even though clicking on other model orders often gives slightly or notably different mode shapes.

When identification error is actually addressed [9,10], the strategy is generally based on statistics and as a result is not applicable to cases where the main error is a form of bias [7]. After showing the classical estimation of modes and residual terms based on known poles which is commonly used in most modal analysis packages, it is shown that the resulting superposition can be used to quantify identification errors and contributions per mode and sensor and resulting analyses are illustrated.

3.1. Frequency domain output error estimation

For test/analysis correlation of mode shapes, the target model usually is a linear time invariant system expressed in the pole residue form with lower and upper residual terms [11,21]

$$\left[H_{id}(s)\right] = \sum_{j\in\text{identified}} \left(\frac{\left[R_j\right]}{s-\lambda_j} + \frac{\left[\bar{R}_j\right]}{s-\bar{\lambda}_j} \right) + \left[F(s)\right] + \left[E(s)\right] \tag{2}$$

with a sum of modal contributions, characterized by constant residues R_j for the numerators and denominators involving the excitation frequency $s = i\omega$ and the modal pole λ_j. Residual terms are the flexibility $\left[E(s)\right]$ and inertia $\left[F(s)\right]$ that are characteristic of the transfer being considered. High frequency modes contribute a constant for displacement measurements and a $\left[E\right]s^2$ contribution for acceleration, low frequency modes contribute a $\frac{\left[F\right]}{s^2}$ for displacement measurements and a constant contribution for acceleration.

The residues on the numerator of modal contributions

$$\left[R_j\right] = \left\{c\psi_j\right\}\left\{\psi_j^T b\right\} \tag{3}$$

are the product of observability $\left\{c\psi_j\right\}$ and controllability $\left\{\psi_j^T b\right\}$. Models where these terms are distinguished are in the modal model rather than pole/residue form. In the literature [19,21], the residue R_j is often written $\left[A_j\right] = \left\{\phi_j\right\}\left\{L_j\right\}$ where mode shape $\left\{\phi_j\right\}$ and observability $\left\{c\psi_j\right\}$ are thought to be the same and the controllability $\left\{\psi_j^T b\right\}$ is called modal participation factor L_j. The notation proposed in [11] and used here, while less common, emphasizes the duality between inputs and outputs with the similar role of the observation matrix c and command matrix b, that will be used for test/analysis correlation in Section 4.1.

As detailed in [21], this model is a linear function of observability and residual terms for known controllability and poles so that minimizing the frequency domain distance leads to a maximum likelihood estimation provided that variance information is used. Building of the initial mode set is obtained from poly-reference Least Squares Complex Frequency algorithm (pLSCF) in [21] and sequential narrow-band estimation in [11,12].

Assuming the controllability to be known is not a necessity. For known poles, the missing terms of the pole-residue model are estimated [11] as solution of the linear least-squares problem minimizing the objective function

$$J(R_j(\lambda_j), E, F) = \left| \left[H(s)\right]_{test} - \sum_{j=[1,NM]} \left(\frac{\left[R_j\right]}{s-\lambda_j} + \frac{\left[\bar{R}_j\right]}{s-\bar{\lambda}_j} \right) + \frac{\left[F\right]}{s^2} + \left[E\right] \right|^2 \tag{4}$$

A further step is then needed to extract observability and controllability as detailed in [22] from the residue R_j, but this is thought by the authors to limit bias in the estimation.

In most applications, transfers are measured for multiple input/output pairs. The approach is fairly standard and very efficient even for a problem where transfers are considered at many actuator/sensor pairs. It is however quite sensitive to errors on the position of poles so that non-linear optimization of the poles, while not very common [11,21], is very helpful.

3.2. Mode and sensor contributions to the identification error

The objective function, see Eq. (4), while largely used, is not typically analyzed in detail. Perfect identification is obtained if test and identified transfer functions are perfectly superposed. Graphical superposition is often used, but cannot be exploited for more than a few transfers, so that other tools are proposed here.

It is useful to note that the objective function (4) is obtained as a sum of positive contributions associated with sensor/actuator pairs (columns of H that will be indexed c in the following) and retained frequencies (rows of H).

The contribution of a mode is well known to be maximal around its resonance. A classical method is to focus the identification on the half power bandwidth (or -3 dB band) given by $\left[\omega_j(1-\zeta_j)\ \omega_j(1+\zeta_j)\right]$ with ω_j the resonance frequency and ζ_j the modal damping. It is thus proposed to define an **identification error** for mode j and input/output pair c by

$$e_{j,c} = \frac{\int_{\omega_j(1-\alpha\zeta_j)}^{\omega_j(1+\alpha\zeta_j)} |H_{Test,c}(s) - H_{id,c}(s)|^2}{\int_{\omega_j(1-\alpha\zeta_j)}^{\omega_j(1+\alpha\zeta_j)} |H_{id,c}(s)|^2} \tag{5}$$

where α is a bandwidth scale coefficient, with $\alpha=1$ corresponding to the -3 dB bandwidth and 5 a relevant value used in [12] and in this paper. This error can be viewed as a numerical evaluation of the quality of the historical "circle fit" method for each input/output pair. It may be noted that for closely spaced modes, the bands may overlap leading to no change in formulation but somewhat harder interpretations.

Fig. 4 illustrates a simple case for the mode at 4050 Hz near the center of the band. On the left, the measurement in light blue is noisy and the match with the identification in dashed red cannot be good. This is coherent with an error (see Eq. (5)) computed at 30%. On the right, the resonance is quite visible and the match nearly perfect, which is well diagnosed by an error of 0.4%. The use of the criterion for all sensors will be addressed in Section 3.3.

In most applications, and especially for 3D laser measurements, high error is expected close to nodes of vibration. To avoid focusing on such transfers, the **level** of a transfer near a given mode is defined to be the mean square value around the target resonance relative to the maximum mean square value over all actuator/sensor pairs

$$L_{j,c} = \frac{\int_{\omega_j(1-\alpha\zeta_j)}^{\omega_j(1+\alpha\zeta_j)} |H_{Test,c}(s)|^2}{\max_c \int_{\omega_j(1-\alpha\zeta_j)}^{\omega_j(1+\alpha\zeta_j)} |H_{Test,c}(s)|^2} \tag{6}$$

Problematic sensors are those with high errors and significant levels. Considering error and level separately is not always appropriate as will be illustrated in the post-processing discussion of Section 3.3. The so-called **Noise Over Signal** criterion, obtained by multiplying the error and the level criteria

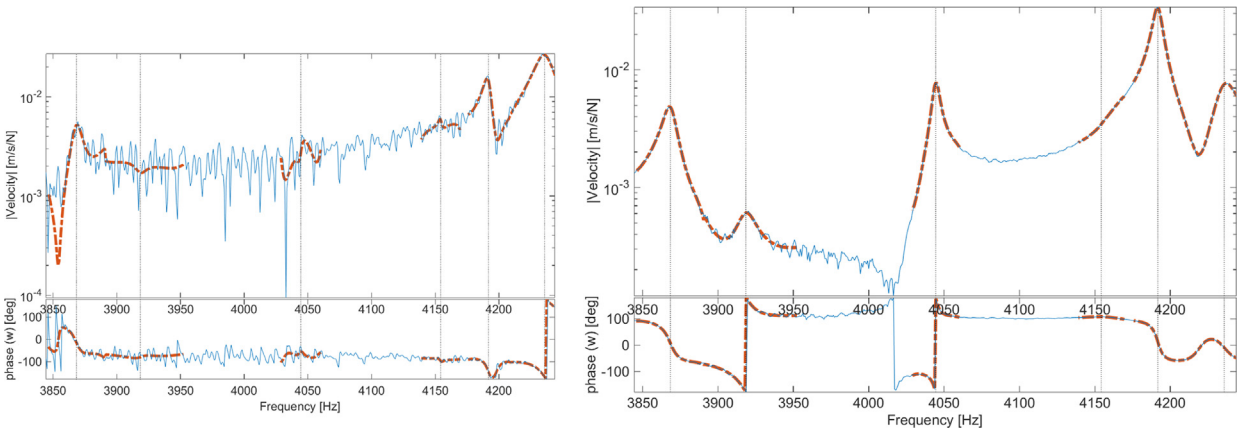

Fig. 4. Sample transfers with high error of 30% (left) and low error of 0.4% (right).

$$NOS_{j,c} = e_{j,c} \times L_{j,c} \approx \frac{\int_{\omega_j(1-\alpha\zeta_j)}^{\omega_j(1+\alpha\zeta_j)} |H_{Test,c}(s) - Hid,\, c(s)|^2}{\max_c \int_{\omega_j(1-\alpha\zeta_j)}^{\omega_j(1+\alpha\zeta_j)} |H_{Test,c}(s)|^2} \tag{7}$$

to focus on transfers where a high error is associated to a high level and as a result more critical. The approximation shown in Equation (7) uses the fact that for a reasonable identification $H_{Test,c}$ and $H_{Id,c}$ should match, so that $\int_{\omega_j(1-\alpha\zeta_j)}^{\omega_j(1+\alpha\zeta_j)} |H_{Test,c}(s)|^2 / \int_{\omega_j(1-\alpha\zeta_j)}^{\omega_j(1+\alpha\zeta_j)} |H_{id,c}(s)|^2 \approx 1$. This approximation illustrates that the product $e_{j,c} \times L_{j,c}$ is close to the ratio of identification error, or noise, and response or signal, hence the NOS denomination retained here.

Fig. 5 (left) shows a sample transfer with high NOS (8.3%): the error is very high 40.4% while the level of 20.5% is significant. The mode is very badly identified (barely visible in the transfer) but the identified residue is of high importance to properly define the mode shape. The existence of locations with high noise for high displacement, indicated by high NOS values, is typical of poorly excited modes. On the right, the transfer also shows high NOS (24.7%) and high error (24.7%) but the mode is very visible (level at 100% since it has the highest amplitude). The high NOS is here due to the bad identification. This specific transfer was measured in a second batch of measurements and a signal processing change led to a damping shift. This example illustrates the fact that the NOS indicator is particularly suited to detect pole shifts often found in batch tests.

For intermediate error levels, two cases are often found: the measurement is noisy but the mode has a sufficient contribution to be identified properly or the contribution of the mode is so small that it cannot be expected to be separated from that of other modes without significant bias.

To distinguish these cases, a last **contribution** indicator is introduced

$$C_{j,c} = 1 - \frac{\int_{\omega_j(1-\alpha\zeta_j)}^{\omega_j(1+\alpha\zeta_j)} |H_{Test,c} - H_{idj,c}|^2}{\int_{\omega_j(1-\alpha\zeta_j)}^{\omega_j(1+\alpha\zeta_j)} |H_{Test,c}|^2}. \tag{8}$$

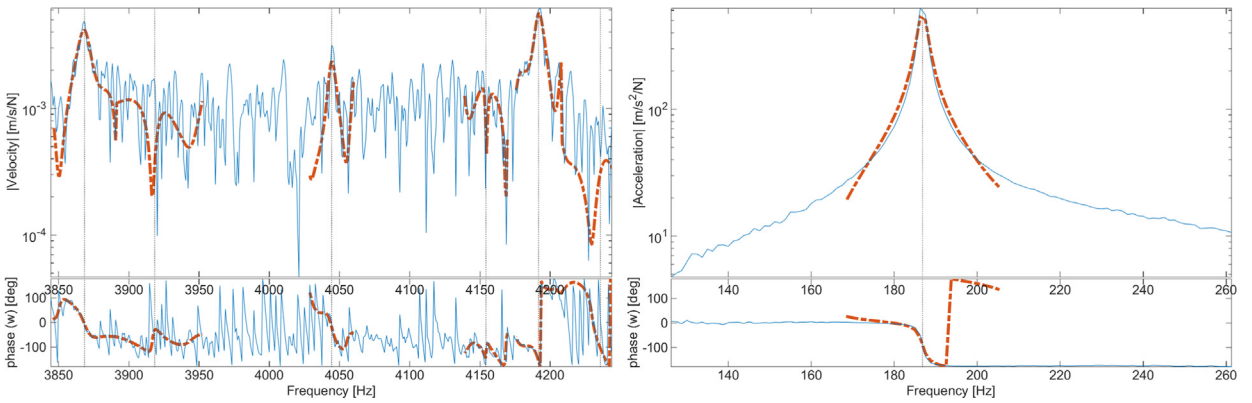

Fig. 5. Sample transfers with high NOS due to bad excitation of the mode (left) and incoherent data (right).

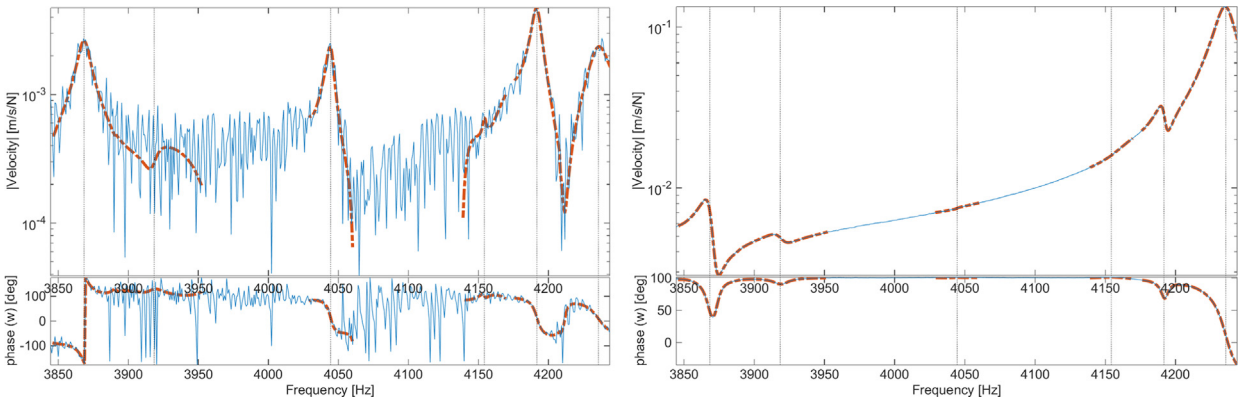

Fig. 6. high error of 18.7% with high contribution of 73.5% (left) and low error of 0.1% with low contribution of 0% (right).

to measure the specific modal contribution of mode j relative to the overall response of all modes in the vicinity of its resonance and give an indication of its *visibility*. For very noisy transfer functions, this indicator can be negative and is then set to 0. The choice of H_{Test} rather than H_{Id} for the normalization is subject to discussion. Using H_{Id} was found to generate false positives, when the estimated contribution is high for very noisy signals even though no proper identification result can be expected. Again for transfers with good identification, the impact should be minimal.

Fig. 6 illustrates transfers, where such discussion is needed. On the left near 4050 Hz, the mode is well visible despite the quite high noise level. It may thus be important to keep it for correlation interpretation. One the right, the figure shows a transfer where the error is very low but the mode shape is not visible at all. The capability to identify the residue well is doubtful since the identification may easily be biased.

The proposed criteria allow for a decomposition of the global identification error into contributions per mode and per transfer. For each mode, obviously problematic sensors with high error, low contribution and low level can be ignored automatically and properly identified results can be kept with high confidence. Intermediate results can then be analyzed in more detail using sorts by level, contribution or NOS to highlight problematic transfers as illustrated in the next section.

3.3. *Post-processing of error, level and contribution*

For practical use, especially in the presence of many sensors, post processing tools, allowing sensor sorting in tables and graphical visualization of criteria is critical and illustrated here.

After identification, a quality table as shown in Table 1 summarizes the results. For each mode, the mean error and the mean contribution are defined as the mean of those two criteria on all the sensors for each mode. This is useful to quickly evaluate the overall quality. The classical Modal Phase Collinearity criterion [23] (quantifying if mode shapes are real) is also computed.

The table is colored using thresholds defined for each criterion, which helps quick evaluation of the overall quality. These thresholds are subject to discussion, but the values used here are

- Error: 0% < 10% < 30% < 100%
- Contribution: 100% > 20% > 10% > 0%
- MPC: 100% > 90% > 10% > 0%

In the present case, modes were identified using an implementation of the pLSCF algorithm. Modes 15, 27, 32, 35, 36 and 37 should be rejected because of the very low MPC: they correspond to numerical modes.

Considering the high number of modes, three of specific interest were selected and their mode shapes are shown in Fig. 7.

Mode #9 is a localized mode shape with high deformation around the center hole. Despite this, the mode is well visible in most transfers. It is very well excited by the impact near the center hole. This is well illustrated by Fig. 8 where most sensors show low error (blue + markers) and high contribution (yellow *o* markers with maximum scaled at 0.5 that is half of Eq. (5) which is found to be a more relevant scale), and the few with higher errors at the right correspond to low response levels (red $\times$ markers with maximum at 0.5), where the measurement is expected to be noisy.

Mode #6 is a much localized mode shape corresponding to the first bending of the cable guide. Error levels in Fig. 9 are significantly above 0.1 for almost 2/3 of the sensors. Nevertheless, the zoom on the first 100 sensors with the lowest error confirms that for relevant sensors where the level is high, the error is very low and the contribution quite high. So the potential of improving results through new measurements is unclear and the choice to discard sensors with high error is confirmed.

Table 1
Quality table of the identification result.

Mode Number	Freq[Hz]	Damp[%]	Error[%]	Contribution[%]	MPC[%]
1	445	0.13	6	75	99
2	457	0.31	13	74	98
3	919	0.37	16	73	99
4	1116	0.14	9	61	98
5	1125	0.09	7	75	97
6	1234	1.44	37	42	99
7	1581	0.12	8	86	100
8	1814	0.07	5	87	99
9	1995	0.08	4	93	99
10	2083	0.09	4	83	99
11	2159	0.06	8	74	99
12	2205	0.09	15	40	95
13	2255	0.14	7	82	99
14	2463	0.19	8	79	98
15	2609	0.08	25	7	1
16	2732	0.14	6	83	96
17	2825	0.07	4	89	99
18	2899	0.06	6	80	99
19	2930	0.06	16	36	98
20	3492	0.17	13	70	97
21	3604	0.11	8	75	99
22	3674	0.11	8	79	99
23	3750	0.21	27	32	92
24	3868	0.11	11	71	98
25	3919	0.17	27	34	94
26	4044	0.06	20	38	92
27	4154	0.03	16	6	2
28	4192	0.07	4	66	98
29	4236	0.17	5	76	99
30	4352	0.08	3	85	98
31	4499	0.23	8	75	99
32	4606	0.04	15	4	3
33	4696	0.06	24	22	90
34	4737	0.14	19	56	96
35	4803	0.09	32	16	10
36	4820	0.05	31	10	7
37	4924	0.04	39	11	5

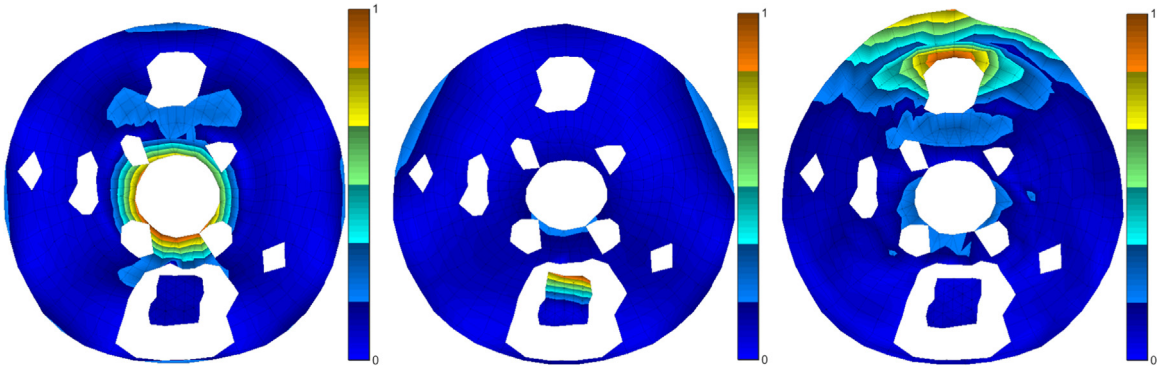

Fig. 7. Modes used for illustrations #9 (left), #6 (middle) and #26 (right). Color proportional to amplitude at test nodes.

Fig. 10 shows, for mode #26, mean error and contribution characteristics similar to mode #6. The mode is much more global and analyzing transfers in more detail shows that many sensors with a significant level (above 10% or 0.05 in the figure due to the 0.5 scaling) also have a high error (usually taken to be 10%).

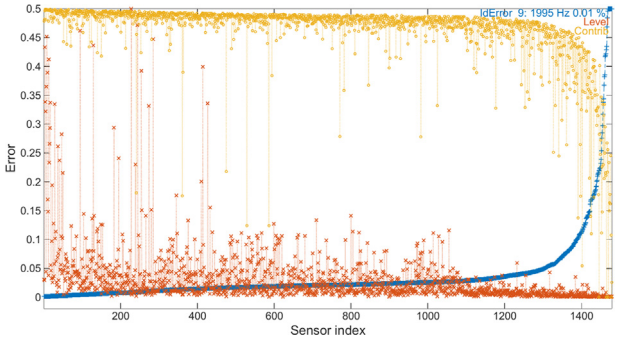

Fig. 8. Error(+), level(x) and contribution (o) for mode #9 as a function of sensor index sorted by error.

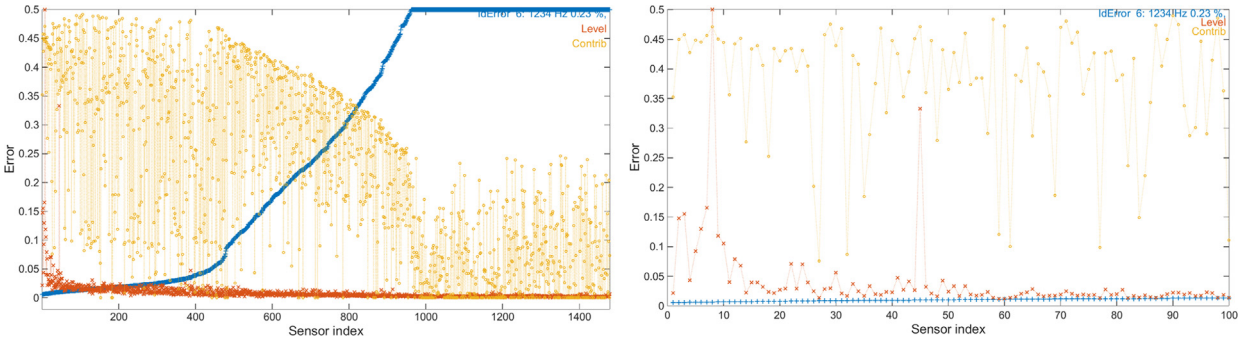

Fig. 9. Error(+), level(x) and contribution (o) for mode#6 (left) and a zoom on first sensors with low error (right).

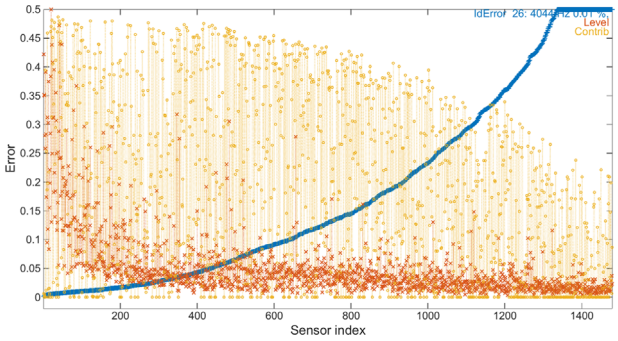

Fig. 10. Error(+), level(x) and contribution (o) for mode 26.

Proper use of the proposed criteria requires navigation tools. The screen capture in Fig. 11 left, shows a top *Modes* table that lets navigate the mode list and a bottom *I/O Pairs* table showing the various criteria for each measured transfer function. In the present case, a single input was retained hence the constant *In*. The *Modes* table shows the test mode indices, frequencies and damping. FEM index, frequency, threshold and MAC values, are also shown and will be addressed in Section 4.3. In the *I/O Pairs* table, sorting is based on NOS and the transfer selected (blue cell in the table) is shown in Fig. 11 right. This figure clearly indicates a poorly excited mode resulting in poor identification quality.

The view by sorted sensors in Figs. 8–10 loses the important information of where these sensors are located. It is interesting to reformat this information as maps in the *x* (horizontal in the figure), *y* (vertical) and *z* (normal) amplitudes.

Error maps for modes #9, #6 and #26 are shown in Fig. 12. Error is much more important for in-plane *xy* (horizontal/vertical in the figure) sensors, especially for modes #6 and #26. This could be expected here because it is well known that with laser vibrometer measurement, noise is higher in the plane relatively orthogonal to the measurement direction. Mode #26 shows in-plane area where the error is low. They correspond to locations where in-plane displacement is important: the relevant signal increases, which explains the lower error. Mode #9 which is very well excited shows a low error even in-plane. Remaining sensors with high error are mostly located where the surface is curved and inclined with respect to the laser direction, which is also known to contribute a lot to poor measurement quality [24].

Contribution maps for modes #9, #6 and #26 are shown in Fig. 13. As expected, mode #9 globally shows a very high contribution. Its contribution map is almost exactly the opposite of the error map which shows that everywhere where

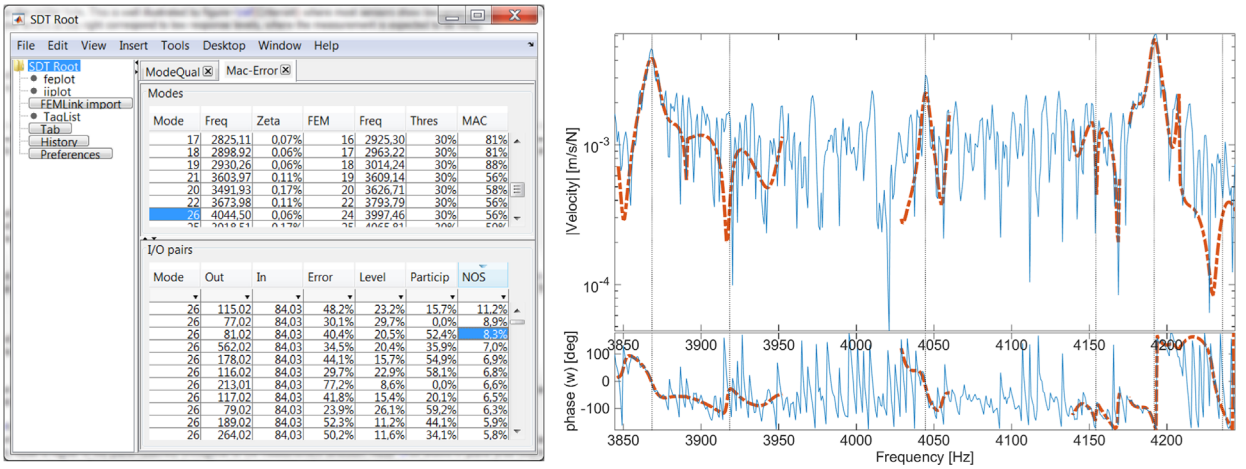

Fig. 11. Left: navigation tables for *Modes* and transfers *I/O Pairs*. Right: selected transfer associated with high NOS for mode #26.

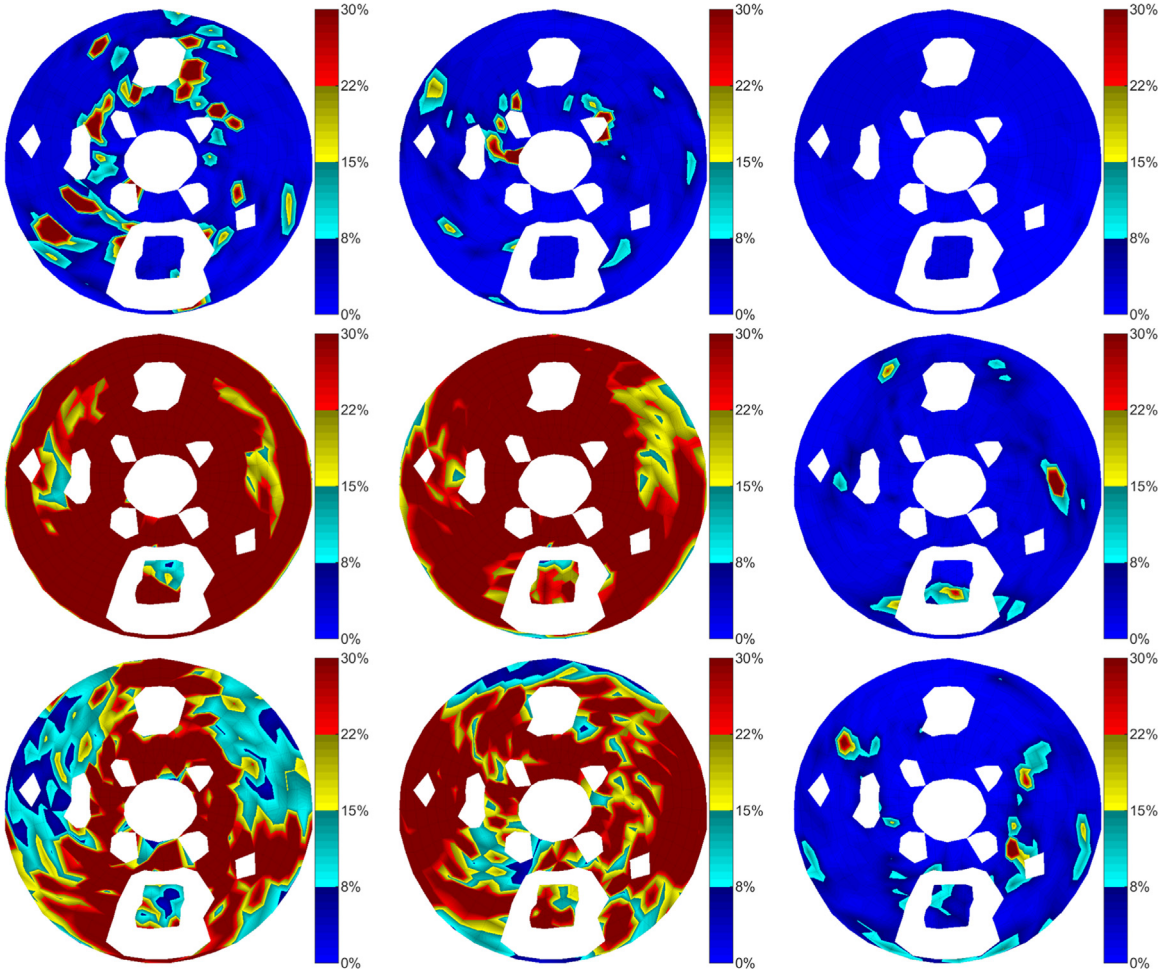

Fig. 12. Error in the *x*, *y* and *z* directions (from left to right) of modes #9, #6 and #26 (from top to bottom).

there is no noise, the mode is well visible in the transfers. For mode #6, areas where the mode shape amplitude is high contribute well. It is the same for mode #26 except around the center hole and close to the top hole, areas where the mode shape amplitude is high but with low contribution, which can be interpreted as areas where the mode is *hidden* by high

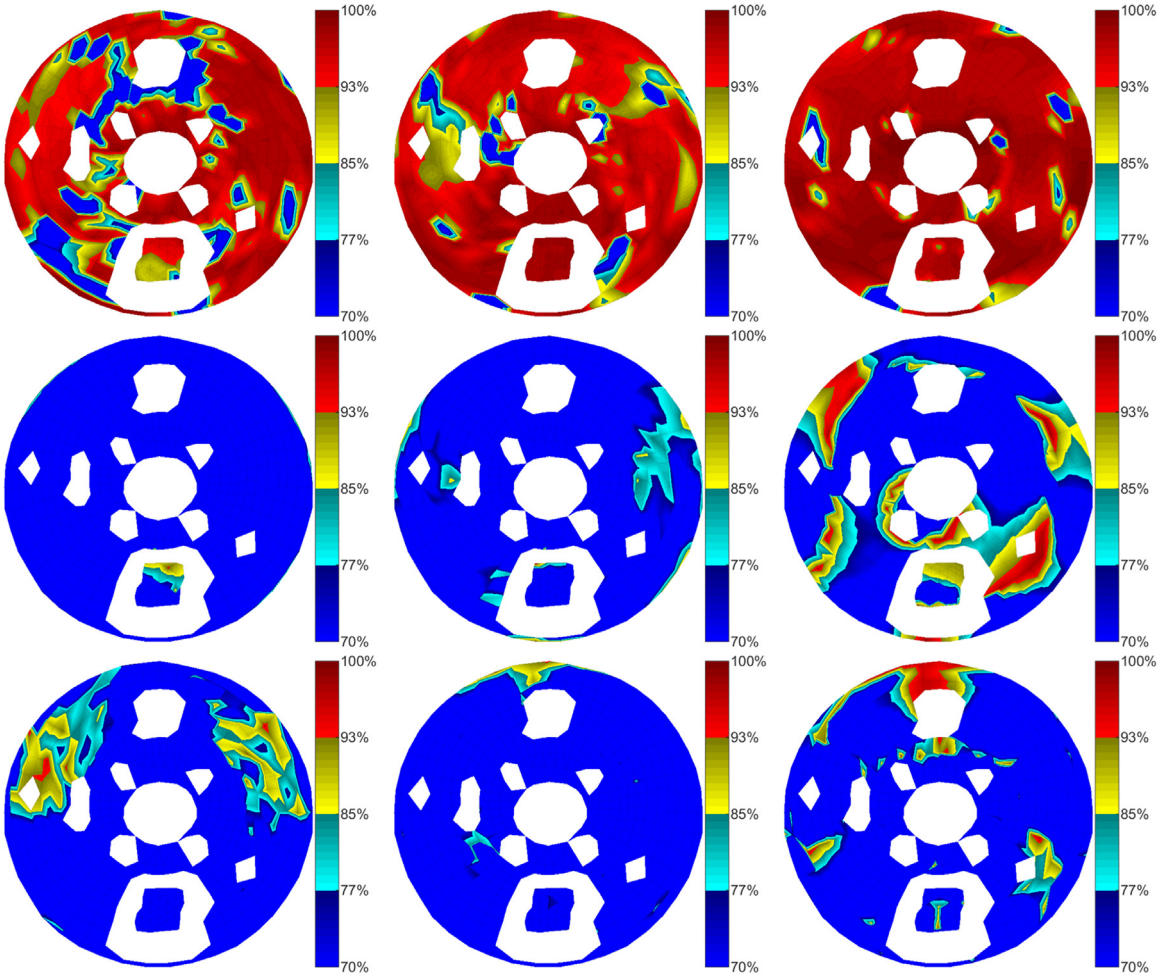

Fig. 13. Contribution in the *x*, *y* and *z* directions (from left to right) of modes #9, #6 and #26 (from top to bottom).

contributions of nearby modes. For these sensors, the capability to properly identify the residue can be questioned since the result is more likely to be biased.

The NOS criterion which was used in the table at Fig. 11 to quickly visualize the associated transfers can also be displayed as a map. In the present case, Fig. 14 clearly highlights problems with mode #26 whereas for mode #6, no badly identified transfers are located at high level locations. The trend is confirmed by animating the identified mode #26 which exhibits unrealistic in-plane displacements.

4. Localization of poor modeshape correlation

When performing test/analysis correlation, the basic inputs are the identification results discussed in Section 3 and the finite element simulation. The first step of correlation is topology correlation, or extraction of FEM motion observed at sensors so that a direct comparison of responses is possible. As illustrated in Section 4.1, this step is often a source of errors.

Given observations, locating sensors contributing to poor correlation is an obvious need and Section 4.2 summarizes existing results from the literature.

The error criterion proposed in Section 3.2 clearly associates a quality with each mode at each transfer (actuator/sensor pair). After the first use in qualifying tests, it is also obvious that the information should be used to allow the distinction between poor correlation due to test or analysis sources as detailed in Section 4.3. It then becomes possible to properly use remaining sensors to localize discrepancies due to modeling as illustrated in Section 4.4.

4.1. Topology correlation for shape observation and MAC

While identification error is the focus of this paper, it is useful to insist on the fact that topology correlation can be a significant source of errors [25]. Since tests are known at sensors, defined by location and direction of velocity

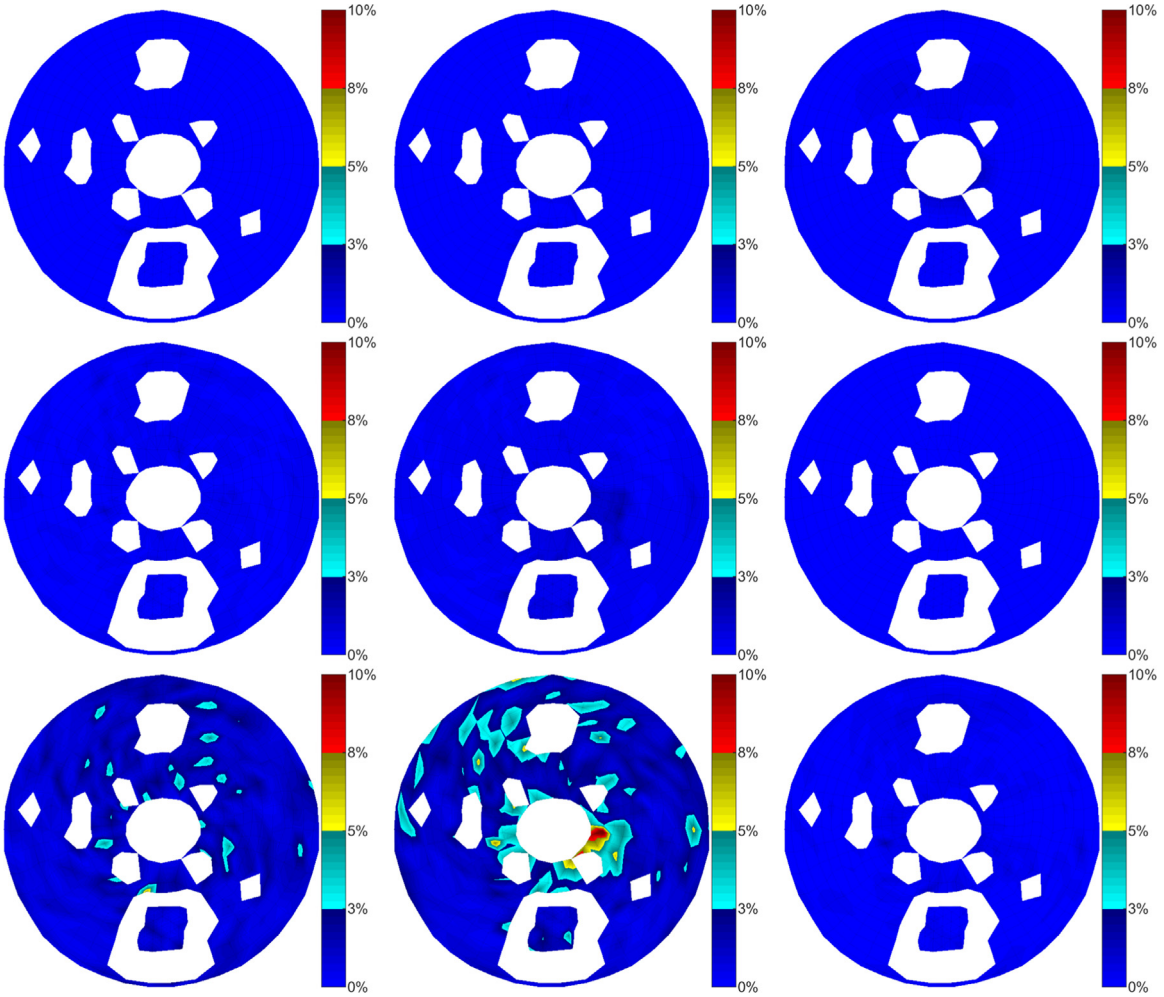

Fig. 14. Noise Over Signal in the x, y and z directions (from left to right) of modes #9, #6 and #26 (from top to bottom).

measurements considered here, and FEM models at Degree of Freedom (DOF), there is a mismatch in the spatial dimensions. The extraction of FEM responses at sensors can be described by an observation equation

$$\{y\}_{NS} = [c]_{NS\times N}\{q\}_N \tag{9}$$

with NS the number of sensors and N the number of DOFs. Outputs $\{y\}_{NS}$ are linearly related to DOF $\{q\}$. The building of the observation matrix $[c]$ is often referred to as topology correlation. Nearest-node and rigid link approximation are the simplest approaches. More accurate strategies use orthogonal projection of the sensor positions to the surface of matching elements and underlying FEM shape functions to properly estimate the motion at sensors. Steps of topology correlation typically involve adjustment of the test-wire frame to match the FEM geometry.

An Iterative Closest Point (ICP) algorithm has been implemented here to optimize the positioning of the test-wireframe over the FEM. Initial positioning is found providing three manually paired nodes from both geometries and optimization is computed. For further details, [26] compares the efficiency of several ICP algorithms, and a fast linearized version of one of them is developed in [27]. Fig. 15 illustrates the topology correlation result of the considered application. The color map shows the distance of each wireframe node to the matched surface through orthogonal projection. The speckle noise aspect of range 0–2.5 mm is linked to the quality of the geometric scanning performed by the 3D-SLDV.

Having identified mode shapes $\left\{c\psi_{\mathrm{id}}\right\}$ (where obviously the observation is physical) and FEM shapes at sensor locations $[c]\{\psi_k\}$, the MAC [1] computes the correlation coefficient given by

$$\mathrm{MAC}_{jk} = \frac{\left|\left\{c\psi_{\mathrm{id}}\right\}^H [c]\{\psi_k\}\right|^2}{\left|\left\{c\psi_{\mathrm{id}}\right\}^H \left\{c\psi_{\mathrm{id}}\right\}\right|\left|\{\psi_k\}^H [c]^H [c]\{\psi_k\}\right|} \tag{10}$$

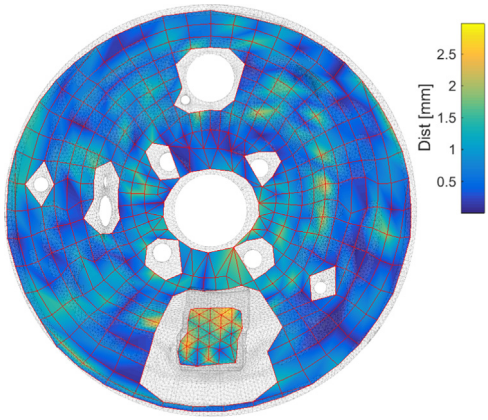

Fig. 15. Sensor matching on FEM.

and thus provides a normalization independent quantification of whether mode shapes are linearly related. A MAC value above 0.9 is typically considered good while a value below 0.7 normally corresponds to poor correlation.

To illustrate the importance of the superposition on the correlation evaluation, Fig. 16 shows on top left the superposition resulting from the three paired points only, and on the top right the superposition after the ICP optimization. Finally, the MAC is computed with the two relative positioning and the bottom of Fig. 16 shows that MAC values for suboptimal superposition are much lower.

4.2. Classical methods for the localization of poor sensors

The need for localization of sensors leading to poor correlation was identified very early and led to different approaches. For the following criteria, identified modeshapes $\{c\psi_j\}$ and observed numerical modeshapes $\{c\psi_k\}$ ($[c]\{\psi_k\}$ will now be written $\{c\psi_k\}$ for convenience) are assumed to be paired. This pairing is classically performed by associating each identified mode shape with the numerical one which is the most correlated (highest MAC value). Then a threshold is applied on the paired modeshapes to keep only those with a MAC value above 70%.

The CoMAC [13] uses the same orthogonality criterion as the MAC, but instead of comparing data of all sensors at each mode shape j, it compares data of all mode shapes at sensor c

$$\mathrm{CoMAC}_c = 1 - \frac{\left\{\sum_{j,k\in Pairs} |c_c\psi_j c_c\psi_k|\right\}^2}{\sum_{j,k\in Pairs} |c_c\psi_j|^2 \sum_{j,k\in Pairs} |c_c\psi_k|^2} \tag{11}$$

where the $1-$ definition is used here to have good correlation for low values of CoMAC. This definition of CoMAC assumes that modes are similarly scaled. As this is sometimes difficult to ensure, a **scaled** CoMAC is computed with shapes $\{c\psi_k\}$ scaled using the Modal Scale Factor (MSF) [28].

$$\{\widehat{c\psi_k}\} = \{c\psi_k\}\mathrm{MSF}_{jk} = \{c\psi_k\}\frac{\{c\psi_k\}^T\{c\psi_j\}}{\{c\psi_k\}^T\{c\psi_k\}} \tag{12}$$

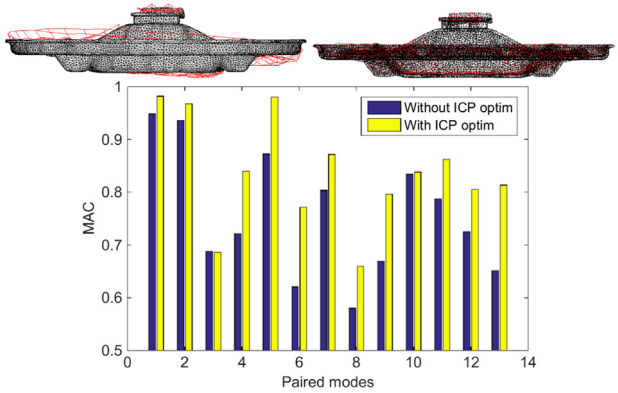

Fig. 16. Superposition of test wireframe over FEM geometry: initialization (top left), ICP optimization (top right) and impact on the MAC (bottom).

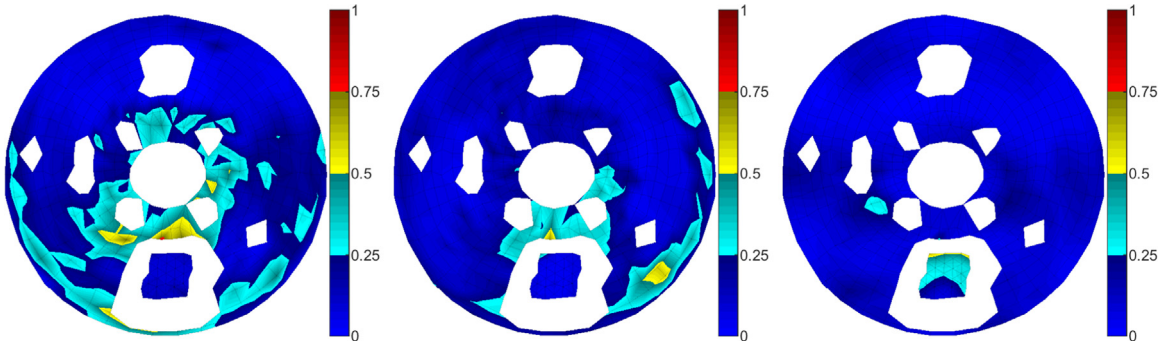

Fig. 17. Scaled CoMAC criterion for the drum brake test case.

which sets the scaling of vector $\{c\psi_k\}$ to minimize the quadratic norm of the difference between $\{c\psi_j\}$ and $\{\widehat{c\psi_k}\}$.

While the CoMAC theory is quite old, the number of papers reporting its use is fairly limited. A reason for this limitation is probably that it needs a high number of identified modes to be relevant in pointing sensors that globally contribute to a poor correlation. The second limitation is due to the global nature of this criterion: as shown in Section 3.3, sensors may have low contributions for a lot of modes (and potentially be badly identified even with a high level), but be very relevant for others (especially local ones). The CoMAC could thus lead to erroneous removal. Fig. 17 shows the scaled CoMAC of the drum brake test case. Many in-plane sensors are found to be a global source of poor correlation which is probably mainly caused by the overall bad in-plane measurement quality, but these sensors may be very relevant for some modes.

The **enhanced** CoMAC (eCoMAC), introduced in [14], uses the mean of the gap between both test and FEM modal amplitudes for each sensor on all modes, despite of the orthogonality criterion. It is given by

$$\text{eCoMAC}_c = \frac{\sum_{j,k\in Pairs} \left\| \frac{\{c_c\psi_j\}}{\|\{c_c\psi_j\}\|} - \frac{\{\widehat{c_c\psi_k}\}}{\|\{\widehat{c_c\psi_k}\}\|} \right\|}{2NM} \tag{13}$$

where the comparison is done using mode shapes that are first scaled using the MSF (to ensure the phase correlation) and then vector normalized to 1 (for the criterion to be between 0 and 1 like the CoMAC). As for the original CoMAC, it needs enough identified modes and works on a global removal of sensors for all modes. Fig. 18 shows the eCoMAC for the drum brake test case. This criterion is defined to be more sensitive to scaling and polarity errors. It points out in the in-plane direction the problem with the sensor close to the cable guide (see explanation below Fig. 20 for details). Nevertheless, in the out of plane direction, it seems that differences between the test and the model are high enough to be detected with the same level at the surrounding of the plate and around the center hole. The eCoMAC is not successful at separating globally poor sensors and sensors which are only problematic for a few modes.

A last criterion, called MAC Variation Technique in [18] or the MAC coordinate criterion (MACCo) in [12], is an iterative algorithm that successively removes sensors that contribute to low MAC values. The structure of the algorithm is detailed in Fig. 19. For a given mode pair j, k and a set of sensors S^n, the MACCo of index $n+1$ is the combination of the MAC value and the set of sensors with one removed from S^n, that leads to the highest improvement of the MAC. The starting value is the MAC computed with all sensors.

Unlike CoMAC variants which require multiple modes, the procedure can be applied by mode (for individual mode pairs) or globally taking the mean MAC over a set of mode pairs.

Iteratively removing sensors and computing the MAC value is very expensive in computation time: for one mode pair,

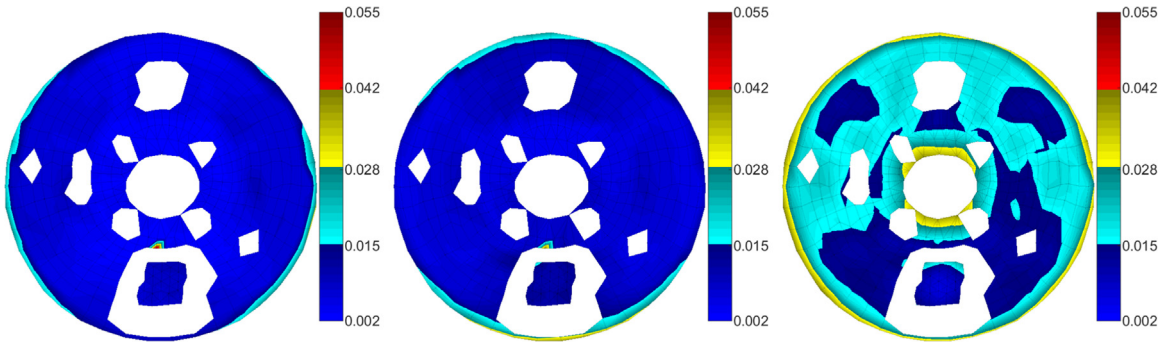

Fig. 18. eCoMAC criterion for the drum brake test case.

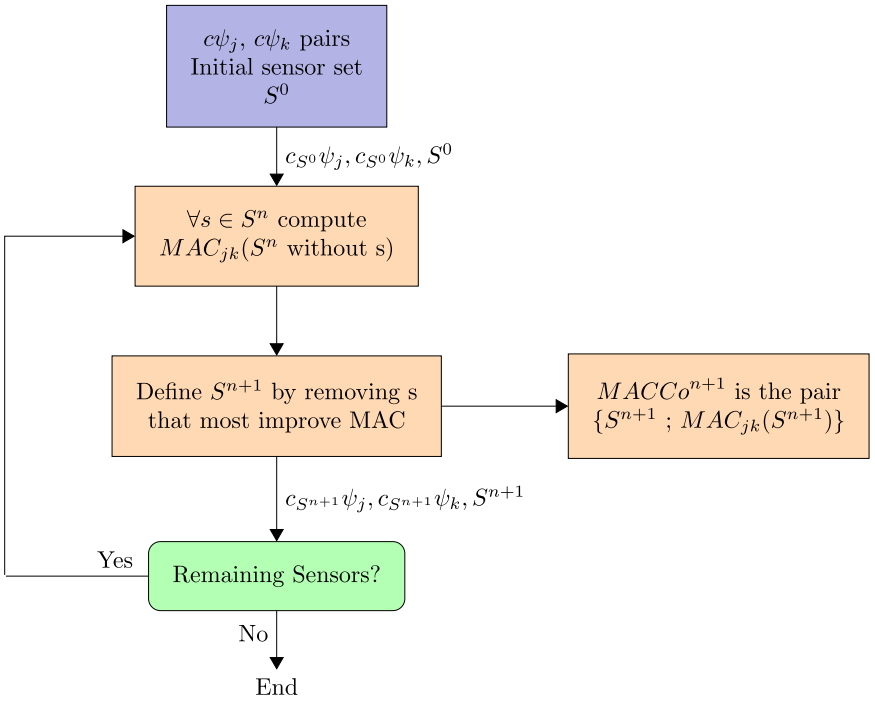

Fig. 19. MACCo Algorithm.

removing a sensor leads to $\frac{s^2}{2}$ MAC computations with s the number of remaining sensors at the considered step. The efficiency can be greatly improved by rewriting the MAC computations for mode pair *jk* with sensor *s* removed as full scalar products with one component removed

$$MAC_{jk}(S^n, s) = \frac{|\left\{c_{S^n}\psi_j\right\}^H \left\{c_{S^n}\psi_k\right\} - (c_s\psi_j)^H(c_s\psi_k)|^2}{|\left\{c_{S^n}\psi_j\right\}^H \left\{c_{S^n}\psi_j\right\} - (c_s\psi_j)^H(c_s\psi_j)|^2 |\left\{c_{S^n}\psi_k\right\}^H \left\{c_{S^n}\psi_k\right\} - (c_s\psi_k)^H(c_s\psi_k)|^2} \tag{14}$$

For example, for the drum brake test case which has 26 paired modes and 1479 sensors, it takes 4 s to compute the MACCo for all paired modes.

4.3. Eliminating test and identification errors from correlation

The main idea of the MACCo is that for each mode pair, a series of sensor eliminations is built and the evolution of the MAC when these sensors are iteratively removed is computed. In the original paper the basis to remove sensors was that it led to poor correlation. With the objective of distinguishing errors on the experimental side, the first obvious objective is the localization of sensors that are generally bad on the test side, typical reasons being: orientation error, scaling error, very noisy measurement on the whole frequency band. Once that is done, a second step is to enhance the confidence in test results and reusing the identification error criteria of Section 3.2 actually seems an obvious step illustrated in this section.

For the objective of detecting sensors globally poorly correlated, multiple strategies are possible. The MACCo algorithm can be applied to the mean MAC of paired modes rather than to each pair individually. The user can then see which sensors come up regularly. Another strategy is to compute the MACCo for each mode pair and then to compute the mean, for all mode pairs, relative evolution of the MAC due to the removing of a specific sensor: this criterion is called *MACevol*.

Fig. 20 shows the result of this global MACevol. Removing sensors 212x and 212y respectively improves the mean MAC of paired modes by 2% and 1%. It corresponds to a node where the laser path was too close to the cable guide. With the little rigid body swinging of the part during the measurement, the laser sometimes hits this cable guide introducing very wrong data: for almost all mode shapes, this sensor shows displacements that are obviously not physical. Looking at the scaled CoMAC at Fig. 17 and the eCoMAC at Fig. 18, both gave these two sensors as a source of poor correlation, but it was mixed with other sensors that reflect global difference in behavior between the test and the model. The MACevol clearly points out these two sensors as the primary source of bad correlation.

Once the global errors have been eliminated, the next step is to ensure increased confidence in test results by eliminating unreliable measurements. For each mode pair, the *MAC-Error* is the evolution of the MAC value for a range of sensor sets of decreasing error levels. A typical result is shown in Fig. 21 for identified modes #9, #26 and #33 associated with their paired numerical modes.

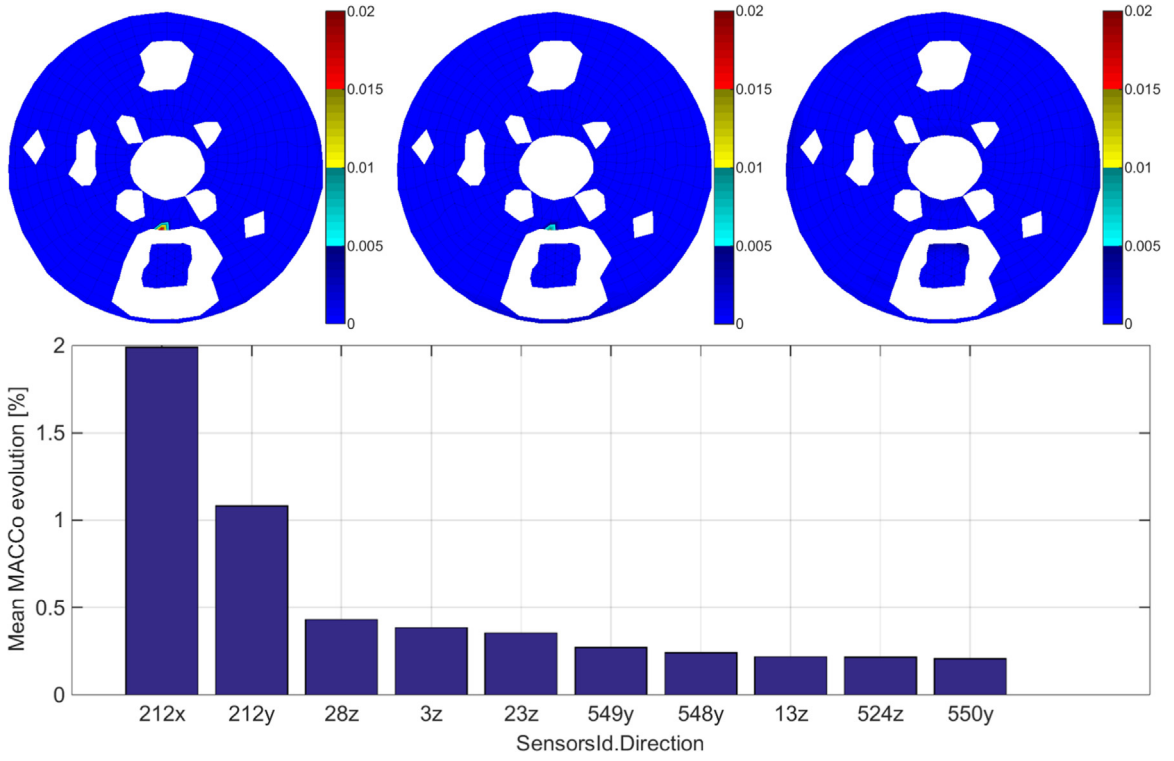

Fig. 20. Mean MACevol: the map in the x, y and z direction (top) and the first ten sensors (bottom).

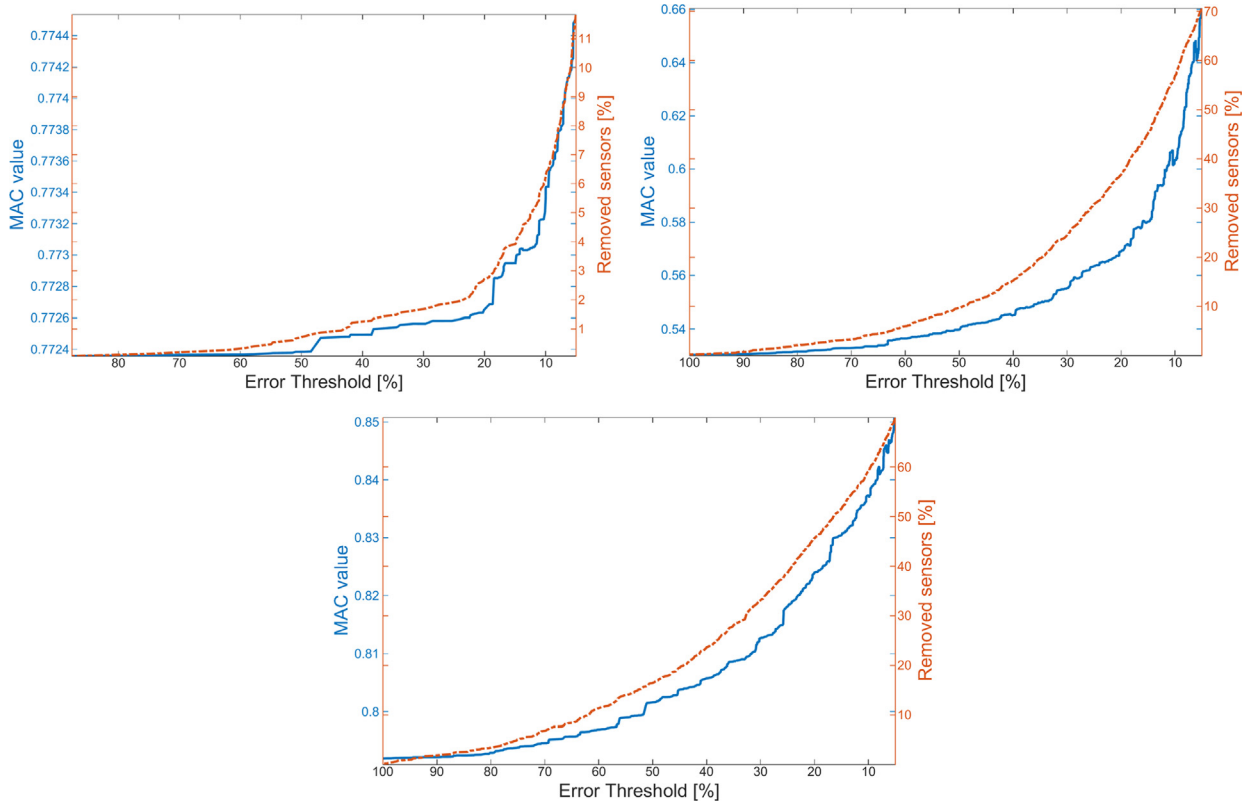

Fig. 21. MACError for identified modes #9, #26 and #33. Blue line and blue left scale gives MAC value. Red line and red right scale gives fraction of removed sensors.

Mode #9 which is very well excited shows no improvement in MAC value with the removal of sensors with the highest error, and very few sensors are removed (below 5% of error) compared to the two other modes. Mode #26 was shown to be badly excited, with a high overall error criterion and a quite high NOS level. Removing sensors with highest error notably increases the evaluation of the correlation: the MAC value is 53% with all sensors and 60% with only sensors whose error is below 10%. Mode #33 is a much localized mode shape where only the surrounding of the part is deforming. Despite a quite good MAC value with all sensors of 79%, removing sensors below 10% noticeably increases this value up to 84%. Removed sensors for modes #26 and #33 are globally located in the in-plane direction.

In the summary tables shown in Fig. 11, the threshold column in the *Modes* tab is used to set the maximum acceptable error value for MAC computations. This value is typically set at 30%.

4.4. Localizing areas of poor correlation

The MACevol was first used to eliminate globally bad sensors. The MACerror then provided a mechanism to eliminate sensors associated with poor identification by setting an error threshold. The results of these two criteria are sensor sets associated with each mode. The remaining information on test mode shapes can then be assumed to be reliable, so that now it becomes relevant to localize sensors where test mode shapes significantly differ from FEM results. This is achieved using the MACCo criterion which can be displayed as a function of the number of kept sensors or as maps of MAC values when a given sensor is removed.

Fig. 22 gives a typical result for mode #9. Before computing the MACCo, a 20% threshold is applied on the MACerror leading to the removal of 3% sensors from the valid test shape. These are visible as a gap at the beginning of the x-axis on top of Fig. 22 and as white color in the map displays.

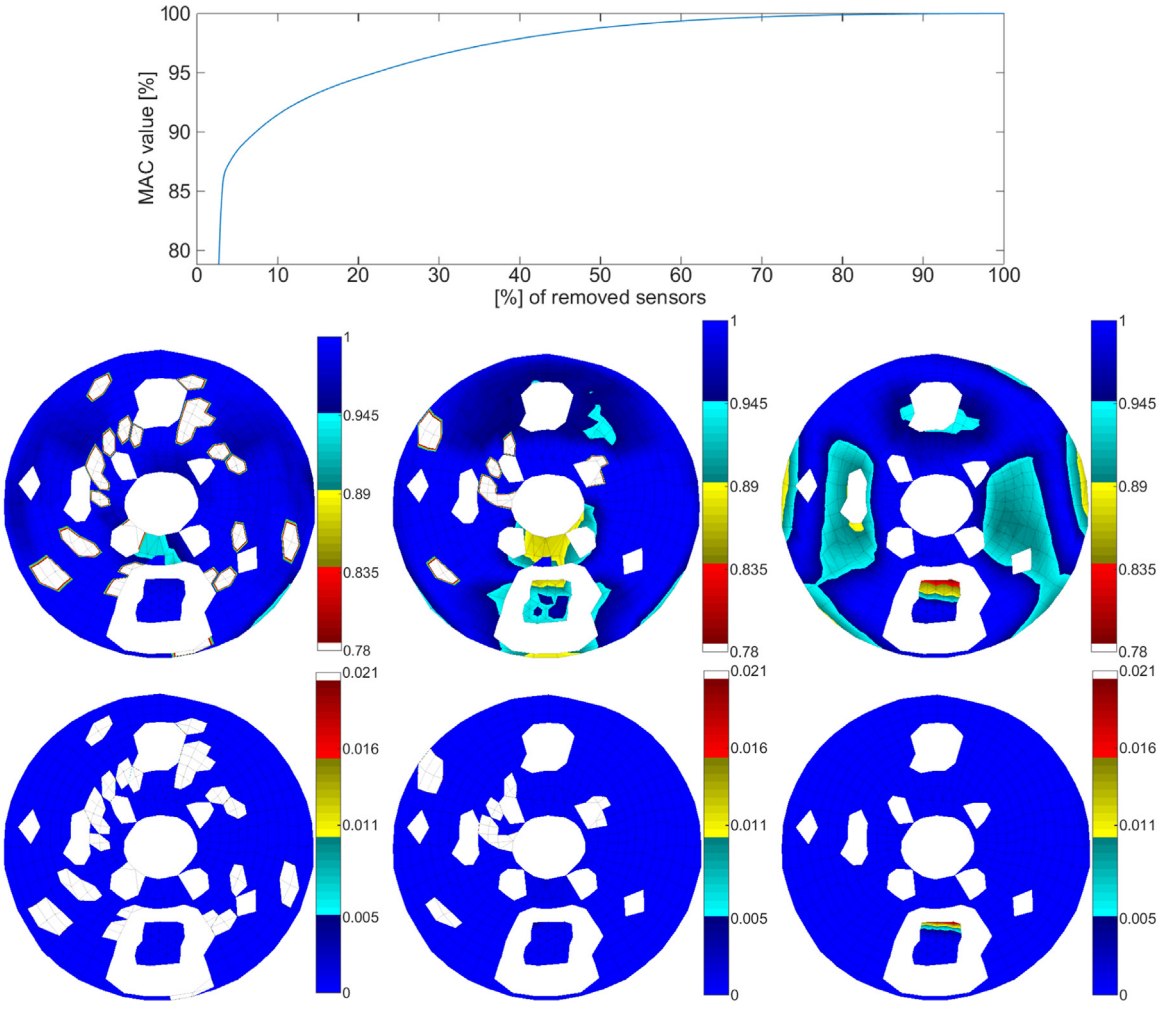

Fig. 22. MACCo displaying for identified mode #9: MAC evolution with sensor removal (top). Display of MACCo value on map (middle) and MACevol (bottom) in x, y and z directions.

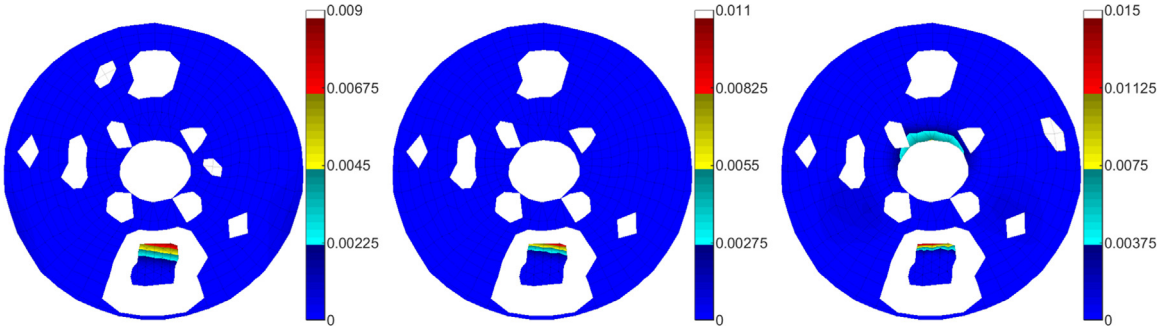

Fig. 23. Relative MAC evolution in the z-direction for modes #3, #7 and #13.

The evolution of the MAC shows a fast increase at the beginning: few localized sensors are contributing very much to the poor correlation. The maps of Fig. 22 indicate that removing the four sensors at the extremity of the cable guide increases the MAC value from 78% up to 88% showing a high difference in behavior between the compared mode shapes.

Rather than showing MAC values associated with various sensors, it is often more readable to localize sensors contributing to a fast improvement of MAC. This is shown as the MACevol criterion (difference of successive MAC values rather than the MAC value itself, see Section 4.2), shown at the bottom of Fig. 22. The removal of each sensor on the cable guide leads to an increase of the MAC of about 2% each. Fig. 23 illustrates that the result is also true for modes #3, #7 and #13, which clearly indicates a modeling issue with the cable guide. In the industrial study, updating of the contact model was considered and shown to be the main error contributor.

5. Conclusion

On the identification side, the paper proposed a strategy to analyze the experimental validity of component mode shapes at each sensor and for each mode. Four criteria were introduced.

- The *error* evaluates the fitting quality of the identified transfer function for each mode and each measured transfer. It is used to compute MAC values with irrelevant sensors removed from mode shapes. This corresponds to the definition of valid sensor sets associated with each mode. Intermediate levels of error (between 10% and 30%) require additional analysis motivating three other criteria on transfers.
- The *level* evaluates the transfer function amplitude of a given transfer in the vicinity of a given mode. It is scaled with respect to the sensor with the maximum amplitude. It is used mostly to ignore other criteria when the amplitude of a given mode is too low and good identification cannot be expected.
- The *NOS* estimates the criticality of the error using a weighting with the level criterion. This criterion is relevant to detect poorly excited modes where transfers with high level do not allow good identification of the targeted mode and cases of poor identification due to shifts in modal properties between measurement batches.
- The *contribution* evaluates the visibility of a mode in the transfer function. This criterion is useful for cases with closely spaced modes and applications where a high level of confidence in the identification quality of specific sensors is needed.

Using table sorting, spatial visualization and interactivity, these criteria are well suited to analyze 3D Scanning Laser Doppler Vibrometer tests with many measurements and provide rapid feedback on the measurement and identification quality. They are very practical tools for the analysis of identification results. The main area needing further work is the extension to MIMO cases, where weighting of criteria for each input will be required.

It may be important to note that the identification was here performed by combining a classical broadband identification with an algorithm such as pLSCF and a narrow band optimization of poles with the IDRC algorithm [11]. The quality of estimated modeshapes is thus quite good to start with. But novel uses based on the proposed criteria are clear perspectives. For example narrow band re-identification of modes keeping only sensors with low error (typically below 10%) and high contribution (typically over 20%) was found to limit bias in the identification of poles. Similarly for mode scaling, the *contribution* can be used to sort collocated sensors and to automatically keep for each mode the best ones to ensure a better identification of the modal mass.

For each mode, the *mean error* evaluates fitting quality; the *mean contribution* the fact that the modal resonance appears as well detached from other modal contributions. The mean error can be used in a fashion similar to the classical MPC which evaluates the complex nature of a mode shape and is expected to be low since very complex modes are rarely found for true, well identified modes.

On the correlation side, the MACCo was shown to be more relevant than the classical CoMAC or eCoMAC. For a given TEST/FEM mode pair, this algorithm sorts sensors by the impact their removal has on a MAC computation. Associated with the sensor sorting, MAC values can be shown for MACCo maps and MAC increase values for MACevol maps.

Combined with the *error* criterion, the MACCo was first used to eliminate unreliable sensors for the shape of each mode by defining a threshold, typically 30%, and the relevance of this procedure was demonstrated. The result is an automatically built sensor set for each mode, allowing removal of irrelevant sensors prior to the evaluation of test/analysis correlation.

Keeping reliable sensors for each correlated mode pair, the MACCo was then used to localize the sources of poor correlation, with the most relevant wire frame representations being associated with MACevol maps. While the localization maps shown here can be exploited directly, it is the author's opinion that using expansion methods such as *error on constitutive relation* [29] or *minimum dynamic residual expansion* [30] will be most efficient at providing further insight on modeling errors.

Acknowledgments

We wish to thank Chassis Brakes International for providing all the experimental measurements used throughout this paper.

References

[1] R.J. Allemang, The modal assurance criterion-twenty years of use and abuse, Sound Vib. 37 (8) (2003) 14–23.
[2] M. Friswell, J. Mottershead, Finite Element Model Updating in Structural Dynamics, 1995.
[3] J.A. Cafeo, R.V. Lust, U.M. Meireis, Uncertainty in mode shape data and its influence on the comparison of test and analysis models, in: Proceedings of SPIE, the International Society for Optical Engineering, 2000, pp. 349–355.
[4] J.A. Cafeo, R.V. Lust, S.J. Doggett, D.J. Nefske, D.A. Feldmaier, S.H. Sung, A design-of-experiments approach to quantifying test-to-test variability for a modal test, in: Proceedings of SPIE, the International Society for Optical Engineering, 1997, pp. 598–604.
[5] J.P. De Clerck, Using singular value decomposition to compare correlated modal vectors, in: Proceedings of SPIE, the International Society for Optical Engineering, vol. 2, 1998, pp. 1022–1029.
[6] T.L. Paez, N.F. Hunter, Statistical Series Part 5 Fundamental Concepts of the Bootstrap for Statistical Analysis of Mechanical Systems, Exp. Tech. 22 (3) (1998) 35–38, http://dx.doi.org/10.1111/j.1747-1567.1998.tb01284.x.
[7] C.R. Farrar, S.W. Doebling, P.J. Cornwell, A comparison study of modal parameter confidence intervals computed using the Monte Carlo and Bootstrap techniques, in: Proceedings of SPIE, the International Society for Optical Engineering, vol. 2, 1998, pp. 936–944.
[8] S.W. Doebling, C.R. Farrar, Estimation of statistical distributions for modal parameters identified from averaged frequency response function data, J. Vib. Control 7 (4) (2001) 603–624.
[9] R. Pintelon, P. Guillaume, J. Schoukens, Uncertainty calculation in (operational) modal analysis, Mech. Syst. Signal Process. 21 (2007) 2359–2373.
[10] E. Reynders, R. Pintelon, G. De Roeck, Uncertainty bounds on modal parameters obtained from stochastic subspace identification, Mech. Syst. Signal Process. 22 (4) (2008) 948–969, http://dx.doi.org/10.1016/j.ymssp.2007.10.009.
[11] E. Balmes, Frequency domain identification of structural dynamics using the pole/residue parametrization, in: International Modal Analysis Conference, 1996, pp. 540–546.
[12] E. Balmes, Structural Dynamics Toolbox (for use with MATLAB), September 1995–2014.
[13] N. Lieven, D. Ewins, Spatial correlation of modeshapes, the coordinate modal assurance criterion (COMAC), International Modal Analysis Conference.
[14] D. Hunt, Application of an Enhanced coordinate modal assurance criterion, International Modal Analysis Conference, 1992, pp. 66–71.
[15] F.N. Catbas, A.E. Aktan, R.J. Allemang, D.L. Brown, A correlation function for spatial locations of scaled mode shapes: (COMEF), in: Proceedings of SPIE, the International Society for Optical Engineering, 1998, pp. 1550–1555.
[16] P. Avitabile, F. Pechinsky, Coordinate orthogonality check (CORTHOG), in: Proceedings of the 12th International Modal Analysis, vol. 2251, 1994, p. 753.
[17] P. Avitabile, T. Foster, Dof selection for smoothing/expansion of measured data., in: the 11 th International Modal Analysis Conference, 1993, pp. 1486–1489.
[18] M. Brughmans, J. Leuridan, K. Blauwkamp, The application of FEM-EMA correlation and validation techniques on a body-in-white, in: Proceedings of the International Modal Analysis Conference, 1993, pp. 646–646.
[19] W. Heylen, S. Lammens, P. Sas, Modal Analysis Theory and Testing, 1997.
[20] D. Ewins, Modal Testing: Theory and Practice, 1984.
[21] M. El-kafafy, T. De Troyer, B. Peeters, P. Guillaume, Fast maximum-likelihood identification of modal parameters with uncertainty intervals: a modal model-based formulation, Mech. Syst. Signal Process. 37 (12) (2013) 422–439, http://dx.doi.org/10.1016/j.ymssp.2013.01.013.
[22] E. Balmes, New results on the identification of normal modes from experimental complex modes, Mech. Syst. Signal Process. 11 (2) (1997) 229–243.
[23] P. Vacher, B. Jacquier, A. Bucharles, Extensions of the MAC criterion to complex modes, in: Proceedings of the International Conference on Noise and Vibration Engineering, 2010.
[24] K.B. Gatzwiller, K.B. Ginn, A. Betts, S. Morel, Practical aspects of successful laser doppler vibrometry based measurements, in: Proceedings of 21 st International Modal Analysis Conference (IMAC-XXI), Kissimmee, Florida. changes in physiological states. Biomedical Signal Processing and Control, vol. 7, 2002, p. 315.
[25] T. França de Paula, G. Rejdych, T. Chancelier, G. Vermot des Roches, B. E, On the influence of geometry updating on modal correlation of brake components., in: Proceedings Vibrations, Chocs & Bruit, 2012.
[26] S. Rusinkiewicz, M. Levoy, Efficient variants of the ICP algorithm, in: 3-D Digital Imaging and Modeling, 2001, in: Proceedings of the Third International Conference on, 2001, pp. 145–152.
[27] K.-L. Low, Linear Least-squares Optimization for Point-to-plane icp Surface Registration, Chapel Hill, University of North Carolina, 2004.
[28] R.J. Allemang, D.L. Brown, A correlation coefficient for modal vector analysis, in: Proceedings of the 1st international modal analysis conference, vol. 1, 1982, pp. 110–116.
[29] P. Ladeveze, G. Puel, A. Deraemaeker, T. Romeuf, Validation of structural dynamics models containing uncertainties, Comput. Methods Appl. Mech. Eng. 195 (4) (2006) 373–393.
[30] E. Balmes, Review and Evaluation of Shape Expansion Methods, International Modal Analysis Conference, 2000, pp. 555–561.